Experimental investigation of the presence of fuel droplets after the passage of a flame front

Romain Thimothée, Christian Chauveau, Fabien Halter, Iskender Gökalp

Experimental investigation of the presence of fuel droplets after the passage of a flame front

Romain Thimothée*[,1], Christian Chauveau[1], Fabien Halter[1], Iskender Gökalp[1]
[1]Institut de Combustion, Aérothermique, Réactivité et Environnement (ICARE), CNRS, Orléans, France
*Corresponding author: romain.thimothee@cnrs-orleans.fr

Abstract
This paper reports fundamental studies of two-phase combustion carried out with mono-sized ethanol droplets aerosol generated with rapid expansion under microgravity conditions. Innovative diagnostics consisting of a coupling laser tomography with a high speed ILIDS technique was successfully applied for aerosol combustion. The droplet diameter reduction together with the radial droplet displacement ahead the flame front has been accurately measured. It was found that the fuel droplets evaporate by following a d^2 law which confirms the validity of this model in an aerosol configuration. Average temperatures of the surrounding gas have been extracted from the ILIDS measurements and were found to be near constant, usually in the range of $600-700$ K, for any aerosol conditions. The laser tomography technique allows the identification of droplets which cross the flame front and then remain in the burnt gases. An experimental diagram has been built using relevant non-dimensional parameters of two-phase combustion to exhibit the observations of droplets passage. The results demonstrated that the droplet size and the droplet interdistance are the most important parameter which control the possibility for the droplet to enter in the burnt gases. Moreover, it was observed that typical topologies of flames in terms of size and number of cells are related to the number density of droplets.

Introduction
Fundamental studies on flame propagation in fuel droplets are essential for a better understanding of many practical applications including spark ignition (SI) engines, gas turbines and industrial furnaces. Real systems of energy conversion contain poly-disperse sprays and turbulent flows which complicates their explorations due to the multiplicity of dependent variables. Usually, deliberately simplified configurations are required. Burgoyne and Cohen [1] was the first to carry out studies on two-phase combustion. They generated a near monodispersed liquid aerosol of tetralin in a diameter range from 7 to 55 μm by bubbling heated nitrogen though tetralin. The mixture was heated to vaporize the tetralin and then passed down a tube where condensation occurs. They identified two separate regimes: for droplet diameters below 10 μm, combustion was similar as in a gas phase, while above 40 μm each droplet burned individually. Later Mizutani and Nakjima [2] examined the effect of adding kerosene droplets in a propane-air premixture. They found that propane flames were markedly accelerated by the presence of kerosene droplets. Hayashi and Kumagai [3] developed a reliable technique to generate near monosized droplets aerosol in a stagnant premixture with the vapor and drops being the same fuel. Then, Hayashi et al. [4] observed the same flame speed promotion for ethanol flames due to the presence of small droplets (4 and 7 μm) and they also showed that, for sufficiently high droplet diameter, two-phase flames develop cellular instabilities on their surface. The same observations have been reported later using the same technique of rapid expansion with experiments of Lawes et al. [5] and also with experiments performed under microgravity conditions in [6, 7].

The presence of a spray considerably complicates the combustion by introducing vaporization process, aerodynamics and mixing processes, heterogeneous combustion with different combustion regimes and can conduct to ignition problems, extinctions and flame instabilities. For example, Atzler et al. [8] observed that the presence of droplets in an iso-octane aerosol causes instability in terms of flame speed oscillation, with periodic fluctuations of flame structure. The cyclic variation of flame speed during flame development has been explained with droplet inertia which induces differences between the speed of droplets and the gas velocity near the flame front. These result with local equivalence ratio variations, which in turn manifest in flame speed oscillations. The equivalence ratio of the gas phase considerably changes and can sometimes conduct to flame extinction. Works of Stapf et al. [9], on modelling spray combustion in Diesel engine, pointed out that group combustion effects have a dominant influence on spray combustion. They showed that large droplets create long stratification in the gas phase which can be inferior to flammability limit while the smaller droplets in group evaporate very quickly generating ignitable premixed fuel$-$air zones. More recently, numerical works of Chen and Han [10] showed that for lean cases and large Lewis number, the presence of fuel droplets significantly increases the minimum ignition power for spherical flames. Bradley et al. [11] demonstrated that, by experimentally assessing the mass burning velocities and entrainment velocities, for sufficient large fuel droplets and richer mixtures, it is possible for droplets to enter the reaction zone and further enhance existing gaseous flame instabilities by significantly increasing the entrained fuel mass flux.

Many studies on spray combustion are present in the literature but the domain still suffers of a lack of experimental data and understanding. The present paper aims to enhance the comprehension of spray combustion domain by specifically focusing on the possibility for fuel droplets to cross the flame front. The evaluation of the state of a spray as fully or not fully evaporated before the arrival of the flame is of prime importance for all internal combustion engines. The objectives are to identify the presence of droplets in the burned gases and to investigate the parameters to be taken into account to correctly predict the potential passage of fuel droplets through the flame front.
Mono-sized and homogeneous ethanol aerosols are generated using the rapid expansion technique [3, 5] in a dual chamber under reduced gravity conditions. High fidelity optical diagnostics are successfully applied to two-phase combustion and new experimental data were measured during combustion (evaporation rate, droplet displacement and droplet diameter reduction). Experimental diagrams are built in order to highlight the relevant parameters of the observed passage of droplets and the possible influence on the two-phase flame instabilities is also discussed.

Experimental setup and procedure

Reduced gravity condition

Reduced gravity conditions were reached in the Airbus A310 ZERO−G of the CNES, during which a 10^{-2}g gravity level is achieved, in order to avoid any disturbing droplet settling effect.

Dual chamber

The experiments were conducted in a pressure-release type dual chamber which consists of a spherical combustion chamber affording a volume of 1 L which is centered in a high pressure chamber of 11 L. The combustion chamber is equipped with 8 evacuation valves, symmetrically distributed, which are calibrated to move under pressure difference effect. The combustion chamber is filled with the flammable mixture while the high pressure chamber is simultaneously filled with nitrogen at the same pressure, thus ensuring proper sealing. When combustion begins, the evacuation valves open and the pressurized gases are evacuated toward the high pressure chamber to be mixed with nitrogen and ensure their totally inert nature. As the high pressure chamber is 10 times greater in volume than the combustion one, the pressure rise inside the combustion chamber due to combustion is dramatically reduced for any initial pressures. This double confinement configuration provides safe operating conditions, especially adequate for microgravity experiments requirements onboard an aircraft. A representative schema of the whole device is given in Figure 1.

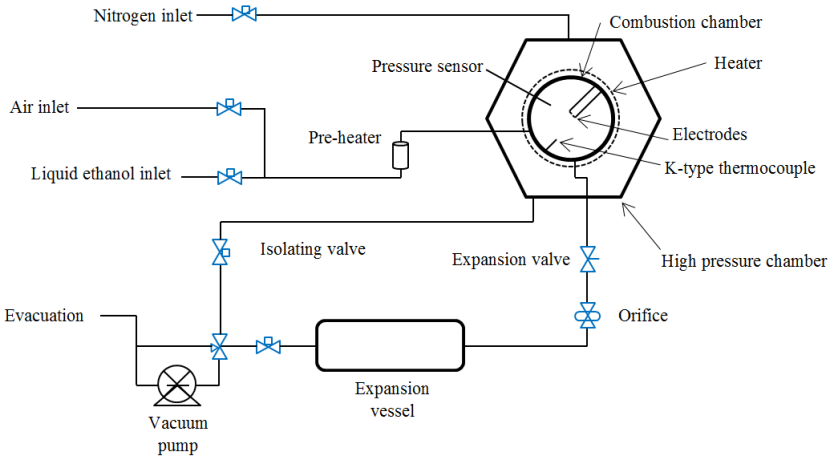

Figure 1. Schematic representation of the whole device.

The liquid fuel injection is performed thanks to a multi-injection system with a switching valve which delivers an accurate volume of ethanol to obtain the targeted equivalence ratio. The fresh gases are heated thanks to an electric heating cable that encircles the chamber. Additionally, a pre-heater is used to pre-vaporize the air-fuel mixture before its arrival in the combustion chamber.

Creation of the fuel aerosol

The fuel aerosol is generated from a gaseous air-fuel mixture, initially prepared in the combustion chamber. The combustion chamber is connected to an expansion vessel of 2.5 L, initially set in vacuum, via an expansion valve and an adjustable orifice (see Figure 1). The opening of the expansion valve induces a fast pressure drop, decreasing the temperature of the gaseous mixture in the combustion chamber. When the partial pressure of the fuel becomes

greater than its saturation pressure, the wet regime is reached, causing start of condensation and so formation of fuel droplets. Once the target pressure of the expansion process has been achieved, the expansion valve closes and two tungsten electrodes centrally ignite the heterogeneous mixture.
A K-type thermocouple of 13 μm in diameter and a pressure sensor running at 1 kHz are placed near-wall in the combustion chamber in order to control the temperature and the pressure during the filling process of the gaseous mixture and measure their variations during the expansion for the aerosol formation (see Figure an example in 2).

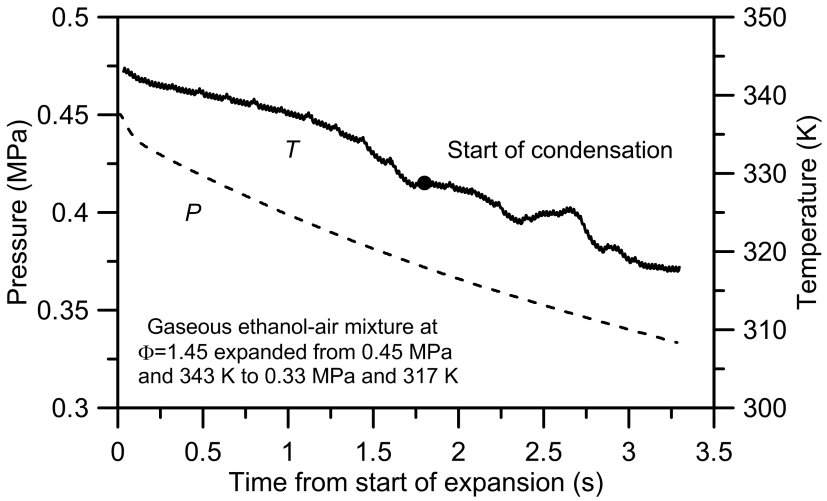

Figure 2. Typical variations in pressure and temperature with time during expansion.

During expansion, only part of ethanol is condensed to form droplets and, at the moment of ignition, ethanol is present both in gaseous state and liquid (droplets). Therefore the equivalence ratio of the mixture can be defined as the sum of a liquid equivalence ratio Φ_l and a gaseous equivalence ratio Φ_g such as: $\Phi = \Phi_g + \Phi_l$. The expansion from a fixed volume into an expansion vessel involves that the total amount of mixture decreases. However it is reasonable to assume that the overall equivalence ratio of the mixture Φ remains constant.

Optical diagnostics

Shadowgraphy system

Two pairs of aligned transparent windows on the two chambers allow optical access. A classical shadowgraph system was employed in order to track the flame front displacement and to visualize the morphology of the flame surface. An Energetiq LDLS is used as the light source and a high speed camera continuously records the flame evolution at 15,000 fps. The temporal evolution of the flame radius $R_f(t)$ is obtained directly from the shadowgraph images where a post-processing program was used to fit the flame front, highlighted by a luminous zone, by a circle. Then the temporal derivation of the flame radius yields the propagation flame speed V_S such as: $dR_f(t)/dt = V_S(t)$. The unstretched propagation flame speed, noted V_S^0, is extracted by extrapolation to zero stretch of values of V_S in function of the flame stretch rate κ using the non-linear model [12, 13] presented in Equation 1,

$$\left(\frac{V_S}{V_S^0}\right)^2 \cdot \ln\left[\left(\frac{V_S}{V_S^0}\right)^2\right] = \frac{-2 \cdot L_b \cdot \kappa}{V_S^0} \quad with \quad \kappa(t) = \frac{2}{R_f(t)} \cdot V_S(t) \tag{1}$$

where L_b is the Markstein length. More details about the methodology of determination of the unstretched propagation flame speed for the present setup can be found in [7].

Coupling of laser tomography and ILIDS

In addition to the shadowgraphy system, two laser diagnostics was used jointly: laser tomography for locating the position and evaluate the velocity of the droplets and an interferometry technique (ILIDS) for determining the droplet size. Both diagnostics require the creation of a planar laser light sheet at the center of the combustion chamber. A laser (Coherent Verdi) emitting a laser beam at 532 nm and of 2.25 mm in diameter was used to an optical system consisting of lenses and a mirror, to generate a thin laser layer of less than 250 μm thick. A light absorber disposed at the bottom of the combustion chamber limits the reflections on the walls. Two high-speed cameras (Phantom v1210 and v1611) are arranged on each optical access for use at high speed during the two-phase combustion process.

a-Laser tomography

A first camera, focusing on the laser light sheet and equipped with an interference filter at 532 nm, receives the light scattered by the fuel droplets which are in the light plane. Fuel droplets are then used as natural tracers and highlight the dynamics of aerosol. An acquisition rate of 19,000 fps and a spatial resolution of 768×768 pixels^2 on a square field of 40.5 mm side enable a precise tracking of the temporal evolution of the position of the fuel droplets during the flame propagation.

b-High speed ILIDS

Interferometric Laser Imaging for Droplet Sizing (ILIDS) is an optical technique for accurately measuring sizes of spherical transparent particles. The reflected and refracted rays from the droplet yield two glare points visible on the focus plane. When these points are imaged out-focus, an interference pattern will become visible with a shape that is determined by the aperture. The angular frequency of this pattern is related to the separating distance between the two glare points and thus to the particle diameter. By using the optical geometric properties [14, 15], it is possible to determine a relationship between the number of fringes N and the diameter of the droplet d such that,

$$d = \frac{2 \cdot \lambda \cdot N}{\alpha} \times \left(\cos\left(\frac{\theta}{2}\right) + \frac{m \cdot \sin\left(\frac{\theta}{2}\right)}{\sqrt{m^2 - 2m \cdot \cos\left(\frac{\theta}{2}\right) + 1}} \right)^{-1} \tag{2}$$

with λ the laser wavelength, m is the ratio of the refractive index of the fuel (ethanol) on the air taken as equal to 1.361, α the angle of collection of light and the scattering angle θ. The latter determines the quality (in terms of contrast) of the light fringes, and is dependent on the implementation constraints on experiment. In this configuration, the axis of the camera was set to $\theta = 90^o$ from the laser plane. The collection angle defines the sensitivity of the technique and depends on the parameters of the camera lenses: $\alpha = 2 \cdot \arctan(d_{lens}/2 \cdot z)$ with d_{lens} the diameter of the receiving lens and z the distance between the lens and the laser light sheet. The determination of the collection angle, and thus the choice of the camera lens, is determined by the range of droplets size to be measured. Reasonable accuracy was obtained with a Sigma lens 180 mm focal length with a lens diameter of 86 mm, positioned at 243 mm from the laser plane. A collection angle of approximately 0.35 radian (corresponding to $\sim 20^o$) was obtained thus permitting a resolution of 1.78 μm/fringe.

The out-focus distance was set to 7.5 mm behind the laser sheet. The acquisition speed was set to 25,000 fps with a spatial resolution of 768×768 pixels^2 on a square field of 28.5 mm side. This allows us, by counting the number of fringes, to access to the measurement of the droplet size decrease in front of the flame front.

Aerosol characterization

Complete two-phase combustion studies require the determination of droplet size and number density (defined as the number of droplets per unit of volume) during the expansion process. The aerosol characterization was performed using a laser diffraction particle size analyzer (HELOS Sympatec) during experiments without combustion. Several measurements are done for each condition of aerosol and the results obtained have shown good cycle to cycle repeatability. Distributions of droplet diameter are recorded and the Sauter Mean Diameter (SMD) is successfully employed as unique diameter to represent the fuel aerosol. The number density, noted N_d,was estimated by measuring the laser attenuation signal and by using the Beer-Lambert law such that,

$$\frac{I}{I_0} = \exp[-\sigma_e \cdot N_d \cdot L] \quad with \quad \sigma_e = \frac{\pi}{4} \cdot \overline{Q_{ext.}} \cdot D_{20}^2 \tag{3}$$

with I and I_0 the intensities of the attenuated and reference laser beam respectively, L the optical path length and σ_e the extinction cross-section defined by [16]. The optical path length was measured from a window to another to 137 mm. The mean extinction efficiency $\overline{Q_{ext.}}$ can be taken to be 1 for uniformly distributed fuel aerosol [17] and the surface mean diameter D_{20}, which is not directly measured by the particle size analyzer, can be reasonably approximated in case of a mono-size droplet aerosol by the arithmetic mean diameter D_{10}.

Figure 3 shows a typical temporal evolution in SMD and number density from start of condensation. Droplet size data and number density for the selection of conditions for combustion experiments were considered only for the period during which values exhibit a constant trend.

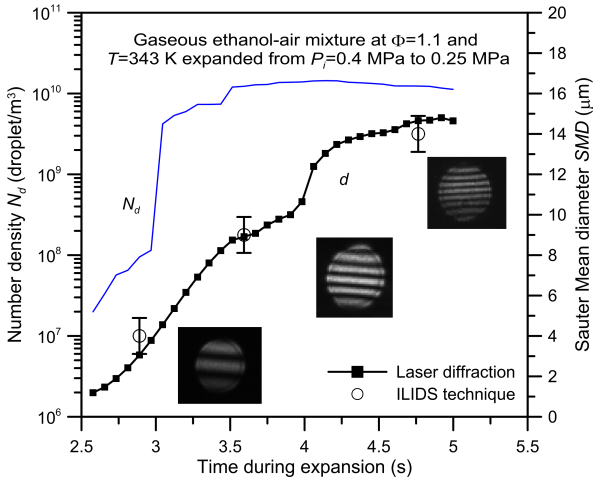

Figure 3. Typical variations of SMD and number density with time during expansion. Validation of the ILIDS technique on the droplet size measurement during expansion.

Droplet diameter measurements were also carried out with the ILIDS diagnostic during the aerosol generating phase. An example of results obtained for the same aerosol generating conditions is plotted in Figure 3. Images of interference pattern are also shown on the graph to illustrate the measurement points. Error bars correspond to the sensitivity of the fringes number on the diameter determination through the calculation of Equation 2. Comparison of the results obtained by the ILIDS technique and those obtained by the laser diffraction particle size analyzer validates the optical system and the method used, and thus demonstrates the ability of the ILIDS technique to measure droplet size in a fuel spray.

Wide ranges of mean diameters and densities of droplets were obtained by varying the initial pressure P_i between 0.35 MPa and 0.6 MPa, the pressure drop, denoted ΔP (the orifice size was kept constant) to reach final pressure from 0.2 MPa to 0.35 MPa and different values for the equivalence ratio from 0.7 to 1.45. Different sizes of fuel aerosols were investigated with average diameters ranging from 5 to 23 μm and densities between $1.5{\cdot}10^{9}$ m^{-3} and $2.0{\cdot}10^{11}$ m^{-3}.

Results and discussion

Measurement of droplet size reduction ahead the flame front

The decrease of the fuel droplets diameter ahead the flame front has been measured by high speed ILIDS for the different cases of studied aerosols. Measurements were performed on several droplets in aerosol, and the arithmetic average diameter D_{10} was used. The temporal evolution of the diameter squared is then calculated and follows a linear trend for all cases of measurement (see example in Figure 4a). This indicates that the evaporation of the aerosol droplets near to the flame front follows the model of d^2 law [18, 19], even for dense cases. Evaporation rate depends on the droplet interdistance [20], which conduct to measure reduced values of evaporation rates in case of highly dense conditions. This inter-distance droplet dependence has been taking into account in the results.

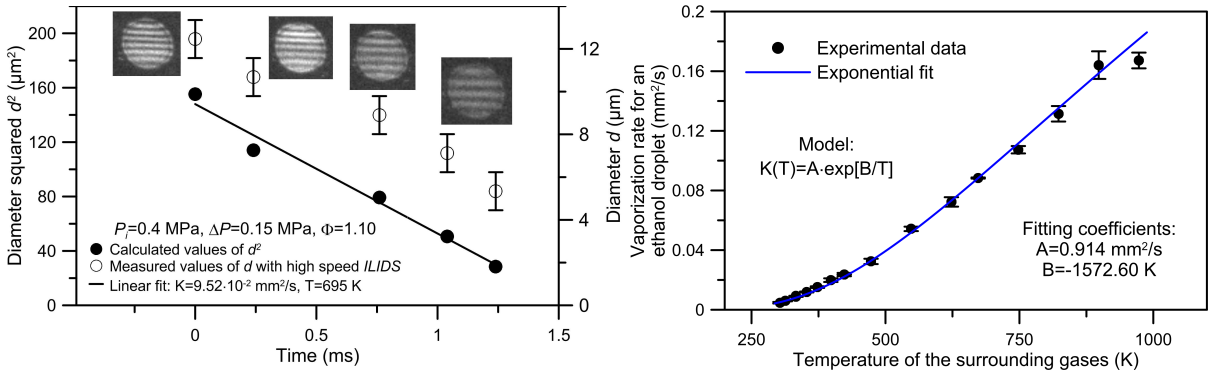

Figure 4. a) Example of a measurement of droplet size reduction ahead the flame front using high speed ILIDS ; b) Temperature dependence on the vaporization rate of an ethanol droplet: experimental data and fitting model [21].

From this droplet size reduction measurements, it is possible to determine the vaporization rate of that drop using the d^2 law. A value of $9.5{\cdot}10^{-2}$ mm^2/s was determinated on example presented in Figure 4a. Values of evaporation rates thus extracted will be used later to estimate the vaporization time of the droplets in the flame front.

Previous experiments conducted on the vaporization of isolated drops, were used to determine a law of variation of the vaporization rate of an ethanol droplet depending on the environmental temperature [21]. This evolution is shown in Figure 4b, and a correlation in the form: $K(T) = A \cdot \exp[B/T]$ can be extracted ($A = 0.91$ mm$^2/s$, $B = -1572.6$ K). By using this correlation, it is possible to determine the average temperature of the gaseous environment (here a value of 695 K for the example shown in Figure 4a). Several temperatures were thus extracted according to many conditions of ethanol aerosols and the results show that all values are between approximately 600 and 700 K. This information indicates that all ethanol droplets undergo a change of state at an average temperature relatively constant. A striking aspect of this result is that, regardless to the aerosol conditions, droplets evaporate in a similar fashion.

Extracted values evaporation rates will be used later to estimate the vaporization time of droplets in the flame front. By taking into account of the uncertainty on the droplet diameter and of the error made by the interpolation calculation (least squared method), the maximum error on the evaporation rate is about 13%, which is acceptable for the present purpose.

Identification of the presence of fuel droplets in the burnt gases

When the flame propagates, fuel droplets, initially motionless, are moved by the expansion of the burnt gases upstream of the flame front. From the images obtained by laser tomography, it is possible to measure radial displacement of each drop in front of the flame front through the application of a PTV treatment (Particle Tracking Velocimetry) on an area corresponding to a crown with a typical width of $4-5$ mm. Three distinct behaviors of droplets ahead the flame were observed. State 0: the droplets evaporate progressively when they are pushed by the expanding gas and do not pass through the flame; State 1: isolated droplets pass the flame and are found in the burnt gas; State 2: the droplets pass through the flame grouped into packet (two to five) and are found in the burnt gas. It is to be noted that the state 1 includes state 0 and that state 2 includes states 1 and 0.

Figure 5 shows examples of radial displacement of the droplets obtained by PTV for the states 0, 1 and 2 for different aerosol conditions. Unlike fresh gases undergoing the expansion of the flame, exhaust gases are at rest. As a result, a particle which passed through the reaction zone may be identified because of its changes in velocity. The presence of drops in the burnt gas is highlighted on the curves by a zero displacement ($dR_d(t)/dt = 0$). The average droplet velocity calculated from the linear part of the curves is also reported on the graph together with the unstretched flame propagation speed of the aerosol flame.

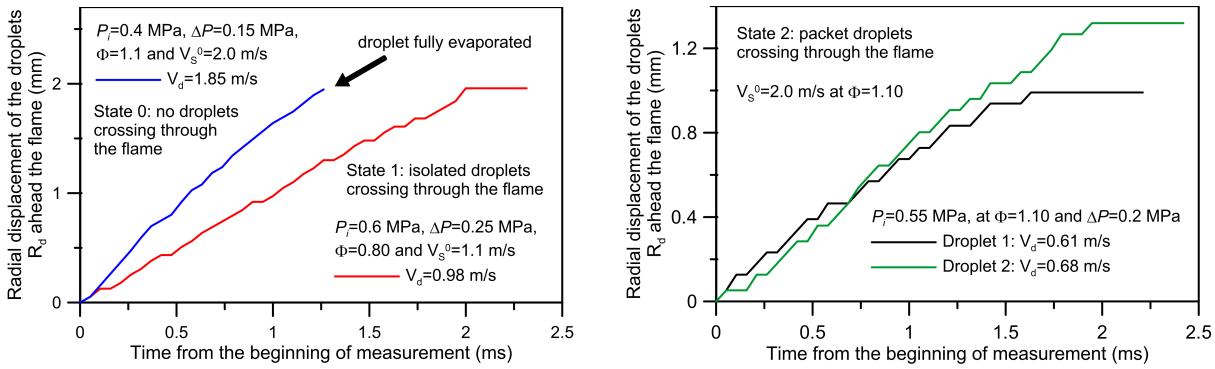

Figure 5. Examples of droplet displacement ahead the flame front for states 0, 1 and 2 at different two-phase conditions.

It is also important to note that the three states observed result in a droplets dynamics that have peculiar characteristics in front of the flame front. When the droplets evaporate with the expansion of gas (state 0), the aerosol movement faithfully follows a circular shape. In state 1, the aerosol behaves analogously to state 0 but with drops that detach from aerosol in an isolated manner. State 2, reveals some packets of droplets that detach from the mist and form an indented aspect. Illustrations of these different observations can be found in Figure 6.

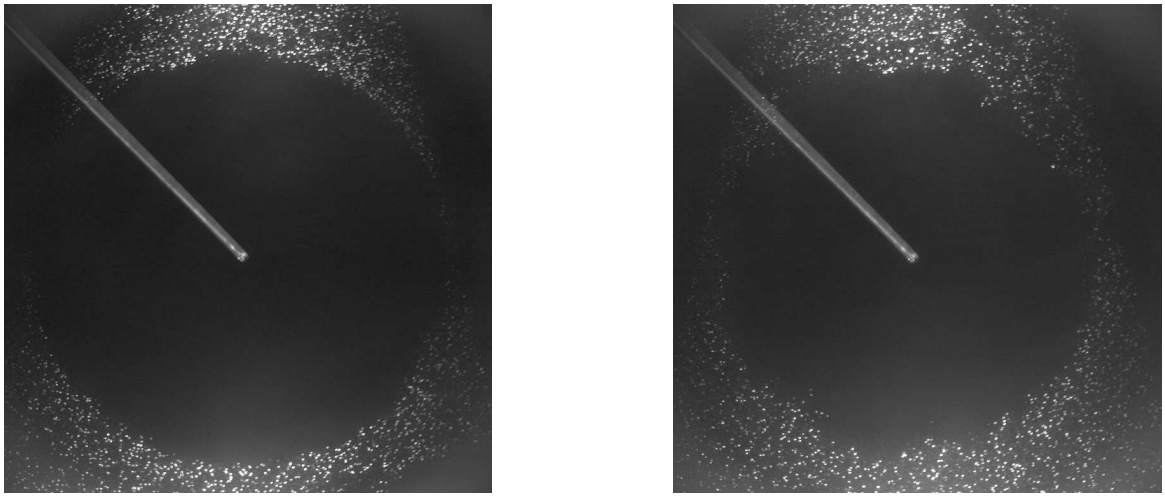

Figure 6. Frames of laser tomography. Left: State 0, no droplets in the burnt gases. P_i=0.4 MPa, ΔP=0.15 MPa and Φ=1.1; Right: State 2, group of droplets in the burnt gases. P_i=0.4 MPa, ΔP=0.15 MPa and Φ=1.4.

Diagrams of experimental observations

The purpose of this section is to use the two-phase combustion parameters measured with the previously described diagnostics to establish an experimental mapping of drops passing through the flame front. Building a diagram involves evaluating characteristic variables which control the phenomenon under consideration. Chui et al. [22] were the first to propose a classification of two-phase flames in terms of burning regime. They demonstrated theoretically the importance of the competition between the evaporation rate and the diffusion rate of the hot gases inside the cloud. These phenomena are directly related to the distance between the drops and their diameter. Later, Borghi [23] proposed a new level of analysis by introducing two characteristic times of the two-phase combustion: the vaporization time τ_v and the chemical time of the flame τ_c. The ratio of these characteristic times can discriminate the droplets state at the proximity of the flame front.

The Sauter Mean Diameter (SMD) values measured by laser diffraction were considered for the droplet diameter of the mist. The droplets interdistance, denoted a, was evaluated using [24]: $a = 1/\sqrt[3]{N_d}$. The chemical time is equal to: $\tau_c = \delta_L^0/S_L^0$ with the laminar flame thickness δ_L^0 and the laminar flame velocity S_L^0. The definition based on the maximal temperature gradient was adopted for the determination of the laminar flame thickness such as,

$$\delta_L^0 = \frac{T_{ad.} - T_u}{\max\left(\frac{\partial T(X)}{\partial X}\right)} \tag{4}$$

with $T(X)$ the spatial profile of temperature, $T_{ad.}$ the adiabatic temperature and T_u the temperature of the fresh gases. The temperature profile was calculated with the PREMIX code and the adiabatic temperature was calculated with the EQUIL code of the CHEMKIN package with the kinetic scheme of Leplat et al. [25] in the aerosol thermodynamic conditions (pressure and temperature just prior ignition) and for the global equivalence ratio of the mixture, Φ. Laminar burning velocity S_L^0 was evaluated based on experimental data of V_S^0 such as, $S_L^0 = \rho_b/\rho_u \times V_S^0$ with ρ_b and ρ_u the respectively density of the fresh and of the burnt gases computed with EQUIL.

The three states of droplet passage are plotted in Figure 7a with in ordinate the ratio a/SMD and in abscissa the chemical time of the flame τ_c. Repeatability of 3 tests was applied on the aerosol combustion experiments. Two confused symbols mean different observation on the three experiments; a single point means three replicates. Figure 7a clearly shows the influence of particle size and density number on the possibility of droplets passing through the flame front. State 3 only appears for values of a/SMD below 15 and the upper limit for droplets to pass the flame front is around 30. It is interesting to note that the chemical time has little influence on the three transition states.

Then the vaporization time was evaluated by considering the d^2 law in the aerosol as: $\tau_v = SMD^2/K$ with K the vaporization rate determined with ILIDS high speed measurements and by applying the correction factor related to the interaction effect between droplets depending on the ratio a/SMD [20]. Results are shown in Figure 7b with the ratio of characteristic times on the x-axis. This second diagram better highlights the three observed states. The state 3 is observed for a/SMD less than 20 and for very large vaporization time versus the chemical time.

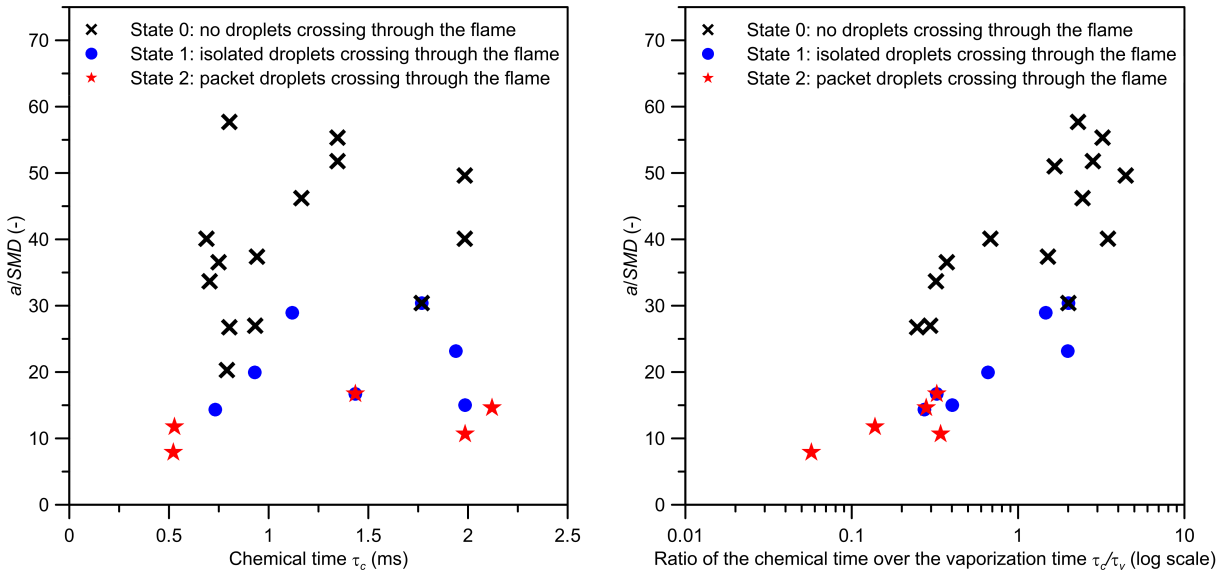

Figure 7. Experimental diagram of presence of fuel droplets in the burnt gases for different conditions of ethanol aerosol in function of a) the chemical time; b) the ratio of the chemical time over the vaporization time (log scale).

Under these conditions, droplets are large and very close to each other. If τ_c/τ_v increases, droplets are more easily vaporized and rarely pass through the flame front. A ratio of $\tau_c/\tau_v > 2$ coupled higher a/SMD value lead to aerosol configurations with small droplets and far-off. Under these conditions, the drops vaporize quickly and have no chance to pass through the reaction zone.
The theoretical limit separating a total and an incomplete evaporation corresponds to a ratio τ_c/τ_v equal to unity. However, experimental observations show that there are several cases identified as state 0 for values of $\tau_c/\tau_v < 1$ (and even close to 0.3) with a/SMD equal to 25. One possible explanation is that the velocity of the droplets is of the same order of magnitude as that of the gas expansion (Figure 5). This velocity will increase the residence time of the droplet before the flame front and thus cause a more significant decrease in its diameter. This phenomenon will depend on the speed of the burnt gas and of the droplet size.

Discussion on the two-phase flame topology

It is well-established that a flame propagating through a fuel aerosol can develop cellular instabilities on its surface [5, 7]. It is so of interest to investigate the relation between the possible presence of fuel droplets in the burnt gases and the topology of the two-phase flames.

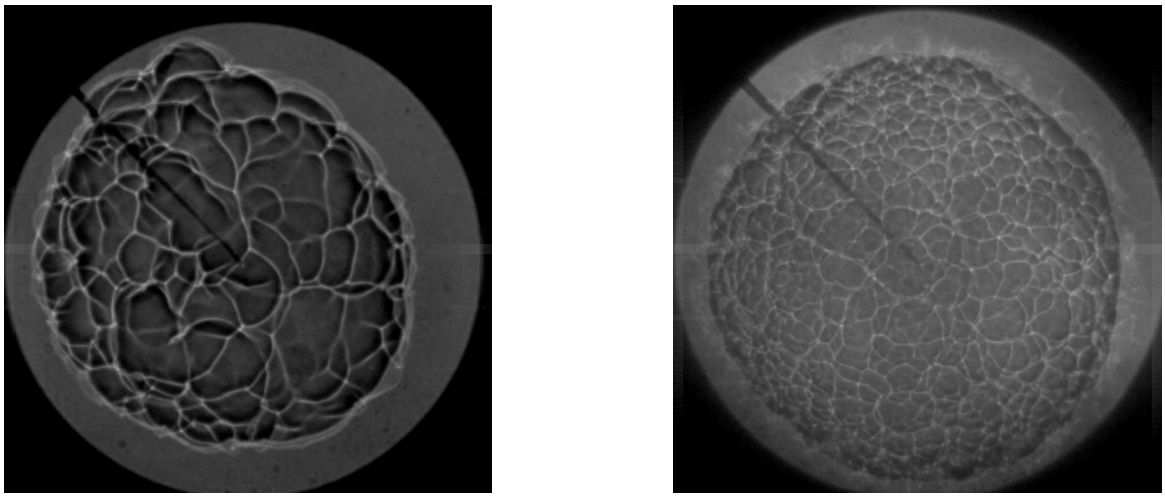

Figure 8. Shadowgraph images of two-phase flames exhibiting two different morphologies. Left: a flame surface with a few large cells at P_i=0.45 MPa, ΔP=0.12 MPa and Φ=1.35 with N_d=2.6·10^{10} m^{-3}; Right: a flame surface with a high number of small cells at P_i=0.55 MPa, ΔP=0.2 MPa and Φ=1.10 with N_d=2.0·10^{11} m^{-3}.

Current results show that flames are cellular when the states 1 and 2 are encountered and flames remains stable and smooth when droplets are fully evaporated ahead the front flame (state 0). This relevant result suggests that the apparition of cellularity in case of a two-phase mixture seems to be related by the passage of droplets in the reactive zone. Different topologies have been observed in terms of size and number of cells on the flame surface and of flame shape. It is found that, in general, flame morphologies with big cells appear for diluted aerosol whereas flame surface with smaller structures, appear for dense aerosol. Examples of flame morphology exhibiting the two kinds of topologies aforementioned are shown in Figure 8. Number density values are also reported and SMD is about the same for the two cases.

Conclusions

Four optical diagnostics were successfully employed in order to measure relevant parameters of two-phase combustion. Specifically, a coupling of laser tomography with high speed ILIDS during two-phase combustion has been validated as a strong tool for the measurement of droplet size reduction ahead the flame front together with their displacement. New experimental data are provided and the main concluding remarks are following:

- The measurement of the droplet diameter ahead the flame front revealed that the vaporization process follows the d^2 law, which confirms the validity of this model for an aerosol configuration, even for dense cases.
- A vaporization rate has been extracted from the droplet diameter measurements and it was found that the vaporization process occurs at a near constant temperature (between 600 and 700 K) for all ethanol aerosol conditions explored.
- Measurements of the droplet displacement allowed identifying, by a zero velocity, conditions for which it is possible for fuel droplets to enter the reactive zone and be present in the burnt gases. Three main droplet states were clearly highlighted: no droplet; isolated droplets and packet droplets in the burnt gases.
- Experimental diagrams were built to exhibit the three states of the droplets against various parameters selected according to common two-phase flame diagrams. It was found that the droplet size together with the droplet interdistance play the major role. An unique criteria of a/SMD =30 was determined to ensure a full drop evaporation before the arrival of the flame.
- Further investigations would be necessary on this point but, current results indicate that cellularities on the two-phase flame surface appear when droplets cross the flame front. Additionally, the droplet inter-distance seems to influence the intensity of the cellular instabilities in terms of number and size of cells.

This work opens several perspectives including a deeper investigation on the evaporation of droplets near the flame front. Calculations on droplet evaporation using the model of d^2 law and by taking into account the displacement of the droplets, the speed of the flame, the temperature profile of the reactive zone with the temperature dependence of the evaporation rate will be conducted in order to provide answers on this aspect.

Acknowledgements

This work was supported by a joint grant from the CNES and the Région Centre. The authors gratefully acknowledge the support of the CNES and the CNRS though the GDR MFA n^{o}2799 for their financial support and the technical support of the parabolic flights.

Nomenclature

Letter

a	droplet interdistance [μm]
d	droplet diameter [μm]
d_{lens}	diameter of the receiving lens (ILIDS technique) [mm]
I/I_0	ratio of the intensity of the attenuated laser beam over the reference one [$-$]
K	evaporation rate of a droplet [mm^2/s]
L	optical path length (laser diffraction particle size analyzer) [mm]
L_b	Markstein length [mm]
m	ratio of the refractive index of ethanol over air [$-$]
N	number of fringes [$-$]
N_d	number of droplets per unit of volume (density number) [m^{-3}]
P, P_i	pressure of the gas, pressure after the filling process and before the expansion [MPa]
$\overline{Q_{ext.}}$	mean extinction coefficiency [$-$]
R_d	radial displacement of droplet [mm]

R_f	flame radius [m]
SMD	Sauter Mean Diameter [μm]
S_L^0	laminar burning velocity [cm/s]
t	time [s]
T	temperature [K]
$T_{ad.}$, T_u	respectively the adiabatic temperature and the temperature of the fresh gases [K]
V_d	mean droplet velocity [m/s]
V_S	stretched flame propagation speed [m/s]
V_S^0	unstretched flame propagation speed [m/s]
X	spatial profile [cm]
z	distance between the lens and the laser sheet (ILIDS technique) [mm]

Greeks

α	angle of collection [radian]
δ_L^0	laminar flame thickness [mm]
ΔP	pressure drop [MPa]
κ	flame stretch rate [s^{-1}]
λ	laser wavelength [nm]
Φ	equivalence ratio of the overall mixture [−]
Φ_g, Φ_l	respectively the equivalence ratio of the gaseous and liquid phase [−]
ρ_u, ρ_b	respectively the density of the fesh gases and of the burnt gases [kg/m^{-3}]
σ_e	extinction cross section [m^2]
τ_c	chemical time [ms]
τ_v	vaporization time [ms]
θ	scaterring angle [radian]

References

[1] Burgoyne, J., and Cohen, L., 1954, *Proceedings of the Royal Society of London A: Mathematical, Physical and Engineering Sciences*, 225, pp. 375-392.
[2] Mizutani, Y., and Nakajima, A., 1973, *Combustion and Flame*, 20, pp. 351-357.
[3] Hayashi, S., and Kumagai, S., 1975, *Symposium (International) on Combustion*, 15, pp. 445-452.
[4] Hayashi, S., Kumagai, S., and Sakai, T., 1977, *Combustion Science and Technology*, 15, pp. 169-177.
[5] Lawes, M., Lee, Y., and Marquez, N., 2006, *Combustion and Flame*, 144, pp. 513-525.
[6] Nomura, H., Izawa, K., Ujiie, Y., Sato, J. i., Marutani, Y., Kono, M., and Kawasaki, H., 1998, *Symposium (International) on Combustion*, 27, pp. 2667-2674.
[7] Thimothée, R., Chauveau, C., Halter, F., and Gökalp, I., June 15.-19. 2015, Proceedings of the ASME Turbo Expo 2015.
[8] Atzler, F., Demoulin, F., Lawes, M., Lee, Y., and Marquez, N., 2006, *Combustion Science and Technology*, 178, pp. 2177-2198.
[9] Stapf, P., Dwyer, H., and Maly, R., 1998, *Symposium (International) on Combustion*, 27, pp. 1857-1864.
[10] Han, W., and Chen, Z., 2015, *Combustion and Flame*, 162, pp. 2128-2139.
[11] Bradley, D., Lawes, M., Liao, S., and Saat, A., 2014, *Combustion and Flame*, 161, pp. 1620-1632.
[12] Tahtouh, T., Halter, F., and Mounaïm-Rousselle, C., 2009, *Combustion and Flame*, 156, pp. 1735-1743.
[13] Kelley, A., and Law, C., 2009, *Combustion and Flame*, 156, pp. 1844-1851.
[14] König, G., Anders, K., and Frohn, A., 1986, *Journal of aerosol science*, 17, pp. 157-167.
[15] Mounaïm-Rousselle, C., and Pajot, O., 1999, *Particle & Particle Systems Characterization*, 16, pp. 160-168.
[16] Bachalo, W., Rudoff, K. and Brena De La Rosa, A., Jan. 11.-14. 1988, 26th Aerospace Science Meeting.
[17] Payne, A. L., Crowe, C. T., Plank, D. R, 1986, *Instrumentation in the Aerospace Industry*, 32, pp. 469-477.
[18] Spalding, D. B., 1953, *Symposium (international) on combustion*, 4, pp. 847-864.
[19] Godsave, G., 1953, *Symposium (International) on Combustion*, 4, pp. 818-830.
[20] Chauveau, C., Halter, F., and Gökalp, I., Aug. 27.-Sept. 1. 2006, 10th International Conference on Liquid Atomization and Spray Systems.
[21] S. Saharin, B. Lefort, C. Morin, C. Chauveau, L. Le Moyne, and Kafafy, R., June 6.-10. 2011, Proceedings of the ASME Turbo Expo 2011.
[22] Chiu, H., Kim, H., and Croke, E., 1982, *Symposium (International) on Combustion*, 19, pp. 971-980.
[23] Borghi, R., 1996, *Lecture series-van Karman Institute for fluid dynamics*, 2, pp. I1-I39.
[24] Aggarwal, S., and Sirignano, W., 1985, *Combustion and Flame*, 62, pp. 69-84.
[25] Leplat, N., Dagaut, P., Togbé, C., and Vandooren, J., 2011, *Combustion and Flame*, 158, pp. 705-725.